Pergamon

PII: S0005-1098(97)00093-9

Automatica, Vol. 33, No. 10, pp. 1819–1833, 1997

Printed in Great Britain
0005-1098/97 $17.00 + 0.00

Nonlinear Tire Force Estimation and Road Friction Identification: Simulation and Experiments*

LAURA R. RAY†

Extended Kalman–Bucy filtering and Bayesian hypothesis selection can be used to estimate longitudinal and lateral tire forces and road coefficient of friction of vehicles on asphalt surfaces.

Key Words—Nonlinear estimation; parameter estimation; extended Kalman–Bucy filter; vehicle dynamics; road friction estimation.

Abstract—This paper applies extended Kalman–Bucy filtering (EKBF) and Bayesian hypothesis selection to estimate motion, tire forces, and road coefficient of friction (μ) of vehicles on asphalt surfaces. The EKBF estimates the state and tire forces of an eight-degree-of-freedom vehicle from vehicle-mounted sensors. The filter requires no *a priori* knowledge of μ and does not require a tire force model. Resulting force, slip, and slip angle estimates are compared statistically with those that result from a nominal analytic tire model to select the most likely μ from a set of hypothesized values. The methods have application to both off-line construction of tire models and development of vehicle control systems that require μ. Both simulation results and results of applying estimation methods to field test data are presented. Simulation results show excellent convergence and accuracy of μ estimates, and results of processing field test data demonstrate the ability to construct useful tire models. Computation and sensor requirements, and robustness of the μ identification algorithm are considered. © 1997 Elsevier Science Ltd.

1. INTRODUCTION

Tire forces and road/tire interface coefficient of friction govern all aspects of vehicle motion and are important to vehicle simulation, handling evaluation, control system design, and safety measures. Nevertheless, tire forces and road friction depend on uncontrollable environmental characteristics, temperature, wear, normal force, tire pressure, and other factors, and are difficult to measure directly. Tire force models are often constructed and verified using machine testing and field test data for vehicle handling qualities (Szostak *et al.*, 1988; Allen *et al.*, 1986). Machine tests directly measure force vs slip or slip angle, but can only approximate the tire/asphalt interface characteristics. Handling quality tests generally measure steady-state (linear) relationships between tire forces and wheel slip or slip angle.

In the absence of transducers to measure road friction and tire forces directly, their values can be inferred from measured data describing vehicle motion. Ray (1995) describes a method of tire force modeling by off-line processing of field test data using an extended Kalman–Bucy filter (EKBF). The EKBF estimates vehicle motion and longitudinal and lateral tire force histories. Individual wheel slip and per axle slip angle histories can be derived kinematically from the state estimate. Longitudinal force vs slip and lateral force vs slip angle histories can be regressed at approximately fixed normal force and vehicle velocity to verify or construct analytic tire models. No prior knowledge of tire characteristics or road conditions is required to implement the EKBF and tire force modeling procedures. In Ray (1995), these techniques were applied to a five-degree-of-freedom vehicle.

With a nominal tire force model available, vehicle models can be used for control system design and evaluation, handling analysis, and computer simulation. However, analytic tire force models are often parameterized using road friction (peak or slide), which is normally required as an input parameter for the tire force model. Figure 1 shows a family of tire force curves at fixed normal force and varying μ for the analytic model of Szostak *et al.* (1988). Both the longitudinal force vs wheel slip and lateral force vs slip angle are generally characterized by a linear region, and a nonlinear region. In the nonlinear region of Fig. 1, if longitudinal slip is perturbed to a higher value, longitudinal force decreases, increasing slip velocity, and forcing slip

*Received 11 September 1996; received in final form 17 March 1997. This paper was not presented at any IFAC meeting. This paper was recommended for publication in revised form by Associate Editor M. Tomizuka under the direction of Editor K. Furuta. *Corresponding author* Professor Laura R. Ray. Tel. + 1 (603) 646 1243; Fax + 1 (603) 646 3856; E-mail laura.e.ray@Dartmouth.edu.

†Thayer School of Engineering, Dartmouth College, 8000 Cummings Hall, Hanover NH 03755, USA.

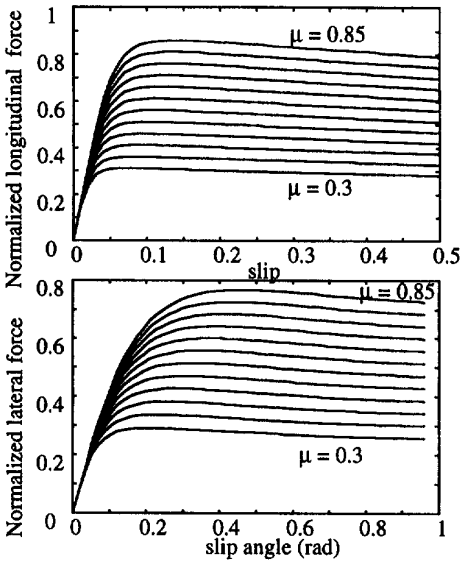

Fig. 1. Normalized tire force curves for $\mu = 0.3$ to 0.85 (increments of 0.05). (a) Longitudinal forces for $F_z = 5600$ N, $\alpha = 0$ rad, (b) Lateral forces for $F_z = 3500$ N, slip = 0.

to increase further; hence, the nonlinear region is unstable, and operation beyond the peak of the force vs slip curve will cause the wheels to lock. Likewise, operation in the nonlinear region of the lateral force vs slip angle curve can cause lateral instability. Control laws for preventing instability, such as those proposed in Taheri *et al.* (1990) depend heavily on tire parameters such as cornering stiffness (slope of the linear region of the lateral force vs slip angle curve), and slip corresponding to peak longitudinal force, which in turn depend on road friction. IVHS emergency intervention systems and driver safety aids require road friction in order to make intelligent decisions (Pape, 1996). In addition to tire force modeling, the EKBF has application to determining unknown road coefficient of friction (μ) in real time. Given an analytic tire force model, the filtered outputs (tire forces, slip, and slip angles) from the EKBF can be statistically compared with those that result from a nominal tire force model to select the most likely μ from a set of hypothesized values.

In this paper, the nonlinear tire force estimation and road friction identification algorithms are described and verified using both computer simulation and processing of field test data. Robustness to reasonable uncertainties in the vehicle parameters and tire force model are considered in the simulation component. Field test data for maneuvers on dry asphalt are processed to examine EKBF performance; to determine the quality of data available for tire force modeling; and to determine μ. The results of processing field test data are also compared to simulated maneuvers for identical inputs, and data extracted for tire force modeling are compared to machine tire test data. Field test data for these tasks were provided by the NHTSA Vehicle Research and Test Center (VRTC) in East Liberty, Ohio.

2. VEHICLE MODEL

An eight-degree-of-freedom vehicle model (Constantine *et al.*, 1991) and analytic tire force model (Szostak *et al.*, 1988) simulate true motion from which noisy measurements are constructed. The equations of motion are

$$\dot{v}_x = v_y r + \frac{1}{m}(-m_s hrp + F_{xf} + F_{xr}), \tag{1}$$

$$\dot{v}_y = -v_x r + \frac{1}{m}(m_s h\dot{p} + F_{yf} + F_{yr}), \tag{2}$$

$$\dot{r} = \{I_{xz}\dot{p} + F_{yf}L_f - F_{yr}L_r + (F_{xfl}\cos\delta_{fl} - F_{xfr}\cos\delta_{fr} + F_{yfl}\sin\delta_{fl} - F_{yfr}\sin\delta_{fr})\frac{t_f}{2} + (F_{xrl}\cos\delta_{rl} - F_{xrr}\cos\delta_{rr} + F_{yrl}\sin\delta_{rl} - F_{yrr}\sin\delta_{rr})\frac{t_r}{2} + M_z\}\frac{1}{I_{zz}}, \tag{3}$$

$$\dot{p} = \{m_s h(\dot{v}_y + v_x r) + I_{xzs}\dot{r} + m_s hg\phi + M_{\phi f} + M_{\phi r}\}\frac{1}{I_{xxs}}, \tag{4}$$

$$\dot{\phi} = p, \tag{5}$$

$$\dot{\omega}_{fl} = (F_{xfl}R_w - T_{fl})\frac{1}{I_w}, \tag{6}$$

$$\dot{\omega}_{fr} = (F_{xfr}R_w - T_{fr})\frac{1}{I_w}, \tag{7}$$

$$\dot{\omega}_{rl} = (F_{xrl}R_w - T_{rl})\frac{1}{I_w}, \tag{8}$$

$$\dot{\omega}_{fl} = (F_{xrr}R_w - T_{rr})\frac{1}{I_w}, \tag{9}$$

where

$$F_{xf} = -(F_{xfl}\cos\delta_{fl} + F_{xfr}\cos\delta_{fr}) - (F_{yfl}\sin\delta_{fl} + F_{yfr}\sin\delta_{fr}), \tag{10}$$

$$F_{yf} = -(F_{xfl}\sin\delta_{fl} + F_{xfr}\sin\delta_{fr}) + (F_{yfl}\cos\delta_{fl} + F_{yfr}\cos\delta_{fr}), \tag{11}$$

$$F_{xr} = -(F_{xrl}\cos\delta_{rl} + F_{xrr}\cos\delta_{rr}) - (F_{yrl}\sin\delta_{rl} + F_{yrr}\sin\delta_{rr}), \tag{12}$$

$$F_{yr} = -(F_{xrl}\sin\delta_{rl} + F_{xrr}\sin\delta_{rr}) - (F_{yrl}\cos\delta_{rl} + F_{yrr}\cos\delta_{rr}). \tag{13}$$

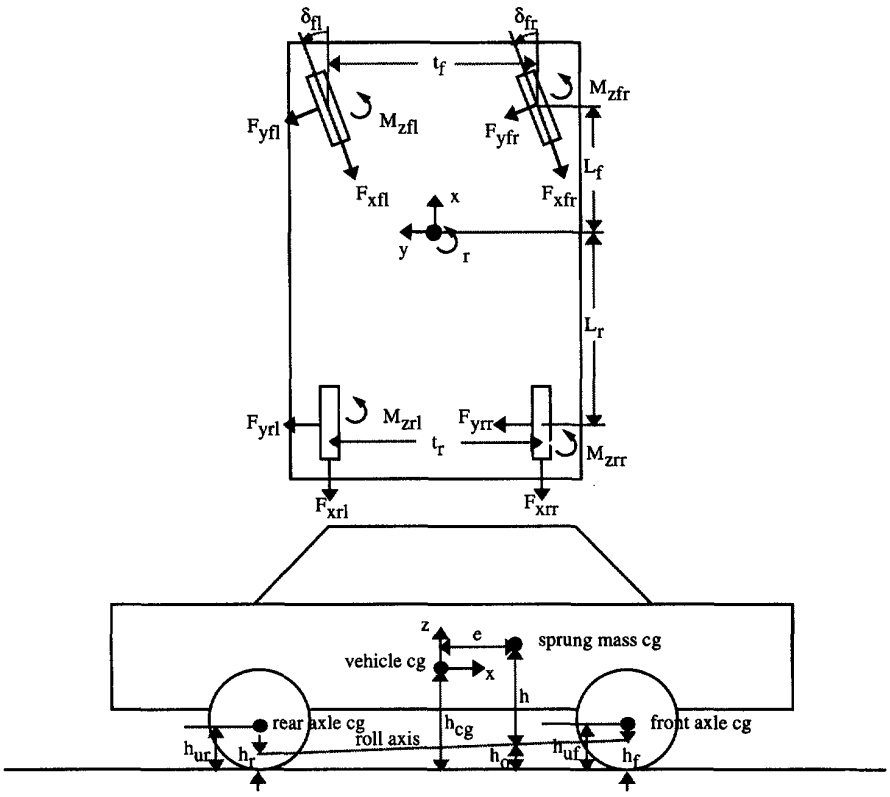

Fig. 2. Sign conventions and parameter definitions for the eight-degree-of-freedom vehicle model.

Table 1. Vehicle simulation parameters (from Constantine et al., 1991)

Parameter	Value	Parameter	Value
Distance, cg to front and rear axle, L_f, L_r	1.2, 1.5 m	Front and rear unsprung mass, m_{uf}, m_{ur}	81.2, 91.6 kg
Distance, sprung mass cg to vehicle cg, e	0.198 m	Vehicle moment of inertia about yaw axis, I_{zz}	2526 kg m^2
Distance: roll axis to sprung mass cg, h	0.183 m	Vehicle product of inertia about roll and yaw axes, I_{xz}	61.7 kg m^2
Front and rear track width, t_f, t_r	1.56, 1.54 m	Sprung mass product of inertia about roll and yaw axes, I_{xzs}	0
Wheel radius, R_w ($= h_{uf}$, h_{ur})	0.32 m	Wheel moment of inertia, I_w	1.07 kg m^2
Front and rear roll center height, h_f, h_r	0.277, 0.017 m	Sprung mass moment of inertia about roll axis, I_{xxs}	489 kg m^2
Sprung mass, m_s	1702 kg		

The state vector $\mathbf{x}(t)$ components are longitudinal and lateral velocity (v_x and v_y) yaw and roll rate (r and p), four wheel angular velocities (ω_{fl}, ω_{rl}, ω_{rl}, and ω_{rr}) and roll angle (ϕ). $\mathbf{u}(t) = [\delta_{fl}\, \delta_{fr}\, \delta_{rl}\, \delta_{rr}\, T_{fl}\, T_{fr}\, T_{rl}\, T_{rr}]^T$ represents steer angles and braking torques at each wheel. Components of the force vector $\mathbf{F}(t) = [F_{xfl}\, F_{xfr}\, F_{xrl}\, F_{xrr}\, F_{yfl}\, F_{yfr}\, F_{yrl}\, F_{yrr}\, M_z]$ are longitudinal and lateral tire forces at each wheel and total tire restoring moment about the yaw axis. $M_{\phi f}$ and $M_{\phi r}$ are roll moments. Sign conventions are defined in Fig. 2; the remaining parameters are given in Table 1. For simulation of vehicle motion, the analytic tire force model of Szostak *et al.* (1988) generates tire forces and moments $\mathbf{F}(t)$ as functions of velocity, μ, and normal force. The model includes roll and compliance steer (Constantine *et al.*, 1991). Roll steer is given by

$$\delta f = \delta f_o + \varepsilon_f \phi, \tag{14}$$

$$\delta r = \varepsilon_r \phi, \tag{15}$$

δf_o represents the commanded front steer angle, which is linearly related to the handwheel angle commanded by the driver. Compliance steer introduces additional steering due to tire forces, moments, and finite suspension compliance. For example, the front wheel steer angles are

$$\delta_{fl} = \delta f + K_{yf} F_{yfl} + K_{xf} F_{xfl} + K_{mf} M_{zfl}, \tag{16}$$

$$\delta_{fr} = \delta f + K_{yf} F_{yfr} - K_{xf} F_{xfr} + K_{mf} M_{zfr}. \tag{17}$$

Table 2. Steering and roll moment parameters (from Constantine et al., 1991)

Parameter	Front	Rear
Compliance steer due to lateral force, K_{yf} and K_{yr}	7.64e-7 rad/N	8.54e-7 rad/N
Compliance steer due to longitudinal force, K_{xf} and K_{xr}	9.44e-6 rad/N	4.5e-5 rad/N
Compliance steer due to moment, K_{mf} and K_{mr}	6.34e-5 rad/N-m	3.61e-5 rad/N-m
Roll steer coefficient, ε_f and ε_r	0.074 rad/rad	0.01 rad/rad
Roll axis torsional stiffness, K_{rf} and K_{rr}	64544 N/rad	48699 N/rad
Roll axis damping, B_{rf} and B_{rr}	2694 N/rad/sec	1063 N/rad/sec

Similar expressions exist for δ_{rl} and δ_{rr}. Table 2 gives the compliance steer coefficients, ε_f and ε_r. First-order braking dynamics, with a time constant of 0.1 s are included. Total brake torque T_b is distributed between front and rear by a proportioning valve.

3. NONLINEAR TIRE FORCE ESTIMATION

Equations (1)–(9) are integrated numerically, adding process noise, and measurement histories are constructed for the EKBF. The measurement equation is

$$z(t) = [r\ \omega_{fl}\ \omega_{fr}\ \omega_{rl}\ \omega_{rr}\ a_x\ a_y\ p]^T = \mathbf{h}[\mathbf{x}(t),\ \mathbf{F}(t),\ \mathbf{u}(t)] + \mathbf{n}(t), \quad (18)$$

where a_x and a_y are longitudinal and lateral acceleration, respectively, and $\mathbf{n}(t)$ is Gaussian, white measurement noise. In addition, the control inputs (handwheel angle and total brake line pressure) are measured, and the relationship between handwheel angle and δf_o is known.

The estimation model includes the equations of motion, but requires no tire force model or knowledge of μ. Instead, tire forces are treated as unknown parameters to be estimated, and the state vector $\mathbf{x}(t)$ is augmented to include differential equations for each force to be estimated. Careful study of equations (1)–(9) shows that all four longitudinal forces and per-axle lateral forces can be determined without requiring direct measurement of tire forces. M_z is neglected in the estimation model. Equations (3), (10)–(13) are modified to replace the individual lateral forces by per-axle forces, and a random walk model is appended to model each force to be determined:

$$\begin{bmatrix} \dot{y}_0 \\ \dot{y}_1 \end{bmatrix} = \begin{bmatrix} 0 & 1 \\ 0 & 0 \end{bmatrix} \begin{bmatrix} y_0 \\ y_1 \end{bmatrix} + \mathbf{w}_y, \quad (19)$$

y_0 represents the force to be estimated, y_1 is its first time derivative, and $\mathbf{w}_y$ is random, white noise. Denoting estimated variables as ($\hat{\cdot}$) and equations (1)–(9) as $\mathbf{f}(x(t), \mathbf{F}(t), \mathbf{u}(t))$, the augmented nonlinear differential equation that models the vehicle in the estimator is

$$\hat{\mathbf{x}}_A(t) = \begin{bmatrix} \hat{\mathbf{x}}(t) \\ \hat{\mathbf{F}}(t) \end{bmatrix} = \begin{bmatrix} \mathbf{f}(\hat{\mathbf{x}}, \hat{\mathbf{F}}, \mathbf{u}) \\ \mathbf{A}\hat{\mathbf{F}} \end{bmatrix} = \mathbf{f}_A(\hat{\mathbf{x}}_A, \mathbf{u}), \quad (20)$$

$$\hat{\mathbf{y}}(t) = \mathbf{h}_A(\hat{\mathbf{x}}_A, \mathbf{u}), \quad (21)$$

$\mathbf{A}$ is a block-diagonal matrix, $\mathbf{x}_A$ is the augmented state vector consisting of the original state vector and forces to be estimated, $\hat{\mathbf{y}}(t)$ is the reconstructed output, and $\hat{\mathbf{F}}$ represents the six estimated forces $[F_{xfl}F_{xfr}F_{xrl}F_{xrr}(F_{yfl} + F_{yfr})(F_{yrl} + F_{yrr})]$ and their first time derivatives. An EKBF is implemented according to the standard algorithm (e.g., Stengel, 1986) by integrating equation (20) and a continuous-time matrix Riccati equation to propagate the state and error covariance estimates, computing the discrete-time filter gain matrix, and updating the state and covariance estimates based on the measurement residual. In the estimator, tire force estimates and steer angle measurement are used to estimate individual wheel steer angles, and the moment contribution to compliance steer is neglected. Filter tuning requires selection of an appropriate disturbance spectral density associated with fictitious noise $\mathbf{w}_y$; "large" values are required for acceptable force transient response. This term was chosen as 250,000 for each term in $\hat{\mathbf{F}}$. Initial values of the state vector can be obtained from transducer measurements prior to application of braking forces, and the error covariance matrix was chosen as $\mathbf{P} = \text{diag}(1\ 1\ 1\ 1\ 1\ 100\ 100\ 100\ 100)$ for the nine elements of $\hat{\mathbf{x}}$. Each element of $\hat{\mathbf{F}}$ was assigned an initial covariance of 10,000 N^2 or $(N/s)^2$. Measurement noise covariance was determined from actual data and transducer specifications.

Slip and slip angle estimates at each wheel are derived from the state estimate. Estimates of slip angles $\hat{\mathbf{a}} = [\hat{\alpha}_{fl}\ \hat{\alpha}_{fr}\ \hat{\alpha}_{rl}\ \hat{\alpha}_{rr}]$ and longitudinal slips $\hat{\mathbf{s}} = [\hat{s}_{fl}\ \hat{s}_{fr}\ \hat{s}_{rl}\ \hat{s}_{rr}]$ are given by

$$\begin{bmatrix} \hat{\alpha}_{fl} \\ \hat{\alpha}_{fr} \\ \hat{\alpha}_{rl} \\ \hat{\alpha}_{rr} \end{bmatrix} = \begin{bmatrix} \delta_{fl} \\ \delta_{fr} \\ \delta_{rl} \\ \delta_{rr} \end{bmatrix} - \tan^{-1} \begin{bmatrix} \dfrac{\hat{v}_y + L_f \hat{r}}{\hat{v}_x} \\ \dfrac{\hat{v}_y + L_f \hat{r}}{\hat{v}_x} \\ \dfrac{\hat{v}_y - L_r \hat{r}}{\hat{v}_x} \\ \dfrac{\hat{v}_y - L_r \hat{r}}{\hat{v}_x} \end{bmatrix}, \quad (22)$$

$$\begin{bmatrix} \hat{s}_{fl} \\ \hat{s}_{fr} \\ \hat{s}_{rl} \\ \hat{s}_{rr} \end{bmatrix} = 1 - R_w \begin{bmatrix} \dfrac{\hat{\omega}_{fl}}{\hat{v}_f \cos \hat{\alpha}_{fl}} \\ \dfrac{\hat{\omega}_{fr}}{\hat{v}_f \cos \hat{\alpha}_{fr}} \\ \dfrac{\hat{\omega}_{rl}}{\hat{v}_r \cos \hat{\alpha}_{rl}} \\ \dfrac{\hat{\omega}_{rr}}{\hat{v}_r \cos \hat{\alpha}_{rr}} \end{bmatrix}, \tag{23}$$

where $\hat{v}_f$ and $\hat{v}_r$ are the estimated magnitudes of the front and rear axle velocities, respectively,

$$\hat{v}_f = \sqrt{(\hat{v}_y + L_f \hat{r})^2 + \hat{v}_x^2}, \tag{24}$$

$$\hat{v}_r = \sqrt{(\hat{v}_y - L_r \hat{r})^2 + \hat{v}_x^2}. \tag{25}$$

4. DETERMINING ROAD COEFFICIENT OF FRICTION

A nominal tire force model can be constructed off-line from EKBF data by regressing force vs slip at fixed normal force and road surface, providing longitudinal and lateral forces as functions of slip, slip angles, normal force, and μ. With a nominal tire force model available, μ can be estimated recursively by statistically comparing the forces estimated by the EKBF to those that result from the tire force model for a particular μ. Given a tire model, denoted $\mathbf{T}(\cdot)$ and its inputs, the outputs, longitudinal and per axle lateral forces, are nondimensionalized by their respective normal forces:

$$\begin{aligned} \mathbf{F} &= [F_{xnfl}\ F_{xnfr}\ F_{xnrl}\ F_{xnrr}\ F_{ynf}\ F_{ynr}] \\ &= \mathbf{T}(\mathbf{s}, \mathbf{a}, \mathbf{F}_z, \mathbf{v}, \mu), \end{aligned} \tag{26}$$

where, for example,

$$F_{xnfl} = \frac{F_{xfl}}{F_{zfl}}, \tag{27}$$

$$F_{ynf} = \frac{F_{ynfl} F_{zfl} + F_{ynfr} F_{zfr}}{F_{zfl} + F_{zfr}}. \tag{28}$$

Denoting $\hat{\mathbf{F}}$ as the tire force estimates, the conditional probability density function of $\hat{\mathbf{F}}$ given μ is

$$\begin{aligned} \mathrm{pr}[\hat{\mathbf{F}}|\mu] &= \mathrm{pr}[\hat{\mathbf{F}}|\mathbf{T}(\hat{\mathrm{s}}, \hat{\mathrm{a}}, \hat{\mathbf{F}}_z, \hat{\mathrm{v}}, \mu)] \\ &= \frac{1}{(2\pi)^{n/2} S^{1/2}} \mathrm{e}^{-1/2(\hat{\mathbf{F}}-T)^{\mathrm{T}} S^{-1} (\hat{F}-T)}. \end{aligned} \tag{29}$$

Equation (29) expresses the probability density of obtaining the forces $\hat{\mathbf{F}}$ given a particular value of μ. $\mathbf{S}$ is an $n \times n$ covariance matrix, and n is the size of vector $\mathbf{F}$. EKBF estimates of slip, slip angle, and wheel velocity, along with normal force estimates at each wheel serve as inputs to the tire force model given an hypothesized μ to compute $\mathrm{pr}[\hat{\mathbf{F}}|\mu]$. Given J hypotheses, at time t_k, the conditional probability of μ_j given $\hat{\mathbf{F}}_k$ is

$$\mathrm{Pr}[\mu_j|\hat{\mathbf{F}}_k] = \frac{\mathrm{pr}[\hat{\mathbf{F}}_k|\mu_j]\mathrm{Pr}[\mu_j|\hat{\mathbf{F}}_{k-1}]}{\sum_{j=1}^{J} \mathrm{pr}[\hat{\mathbf{F}}_k|\mu_j]\mathrm{Pr}[\mu_j|\hat{\mathbf{F}}_{k-1}]}. \tag{30}$$

The most likely value of μ is then given by a weighted sum:

$$\hat{\mu}_k = \sum_{j=1}^{J} \mathrm{Pr}[\mu_j|\hat{\mathbf{F}}_k]\mu_j. \tag{31}$$

The algorithm starts by specifying the J hypothesized values and initial conditional probabilities $\mathrm{Pr}[\mu_j|\hat{\mathbf{F}}_o]$. Equal initial conditional probabilities of $1/J$ represents no prior knowledge of μ. The most likely value is determined by updating the probabilities at each t_k using equations (26)–(31). Static values of normal forces for equation (26) are estimated as

$$\begin{aligned} &[F_{zfl} F_{zfr}] = \\ &\frac{L_r mg - m_s(h + h_o)a_{xs} - m_{uf} h_{uf} a_{xuf} - m_{ur} h_{ur} a_{xur}}{2(L_f + L_r)} \\ &\pm \frac{1}{t_f}\left\{ M_{\phi f} - \frac{h_f m_s}{L_f + L_r}(L_r + e)a_{ys} + m_{uf} h_{uf} a_{yuf} \right\}, \end{aligned} \tag{32}$$

$$\begin{aligned} &[F_{zrl} F_{zrr}] = \\ &\frac{L_r mg + m_s(h + h_o)a_{xs} + m_{uf} h_{uf} a_{xuf} + m_{ur} h_{ur} a_{xur}}{2(L_f + L_r)} \\ &\pm \frac{1}{t_r}\left\{ M_{\phi r} - \frac{h_r m_s}{L_f + L_r}(L_r - e)a_{ys} + m_{ur} h_{ur} a_{yur} \right\}, \end{aligned} \tag{33}$$

where accelerations and roll moments $M_{\phi f}$ and $M_{\phi r}$ are

$$a_{xs} = a_x - r^2 e + rhp, \tag{34}$$

$$a_{ys} = a_y + \dot{r}e - h\dot{p}, \tag{35}$$

$$a_{xuf} = a_x - r^2 L_f, \tag{36}$$

$$a_{yuf} = a_y + \dot{r}L_f, \tag{37}$$

$$a_{xur} = a_x + r^2 L_r, \tag{38}$$

$$a_{yur} = a_y - \dot{r}L_r, \tag{39}$$

$$M_{\phi f} = -K_{rf}\phi - B_{rf}p, \tag{40}$$

$$M_{\phi r} = -K_{rr}\phi - B_{rr}p. \tag{41}$$

In equations (34)–(41), a_x, a_y, r, and p are based on sensor measurements, ϕ is based on the EKBF estimate, and $\dot{r}$, $\dot{p}$ are based on a first-order difference approximation using state estimates. Roll moment coefficients are given in Table 2.

Using the method above, μ estimation is separate from the EKBF, and μ estimation results do not affect state estimates directly. The EKBF provides

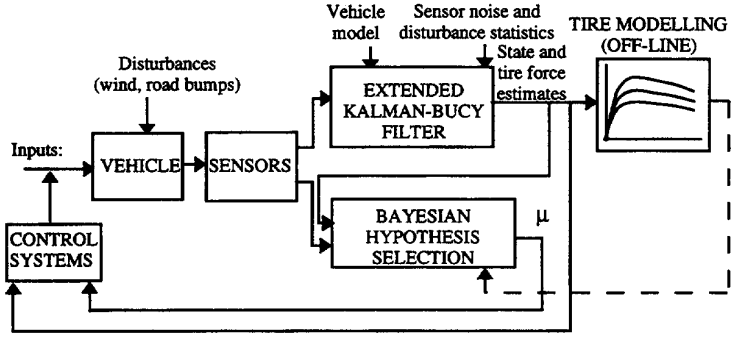

Fig. 3. Procedural block diagram of the proposed EKBF/Bayesian Hypothesis Selection procedures.

state estimates for off-line construction of tire force models, feedback control, and for determining μ. Once μ is estimated, information such as controller setpoints, minimum stopping distance for the road surface, and lateral maneuverability can be determined for decision-making and control. However, because the two tasks are separate, state estimates can be used for feedback before the μ estimate converges. This scenario is vital for good stability and robustness properties. Figure 3 shows a block diagram of the proposed scenario in association with a feedback control loop.

5. SIMULATION RESULTS

5.1. *EKBF evaluation*

Pure steering, pure braking, and combined maneuvers involving both linear and nonlinear tire forces were simulated for evaluation of the EKBF. Tracking ability was determined by simulating a combined maneuver on a road with several sudden changes in μ. Figure 4 shows the results; here, $T_b = 3000$ N m, $\delta f_o = 0.15$ rad, $\mu = 0.3$, $t = [0,0.5)$, $\mu = 0.85$, $t = [0.5, 1.5)$, $\mu = 0.3$, $t = [1.5, 2.25)$, and $\mu = 0.5$, $t = [2.25, 3.0)$ s. The slip, slip angle, and force estimates approximate the actual trajectories well, even in the face of abrupt changes in μ and severely nonlinear tire forces. These trajectories are used below, along with the static normal force estimates to determine μ.

5.2. *Road friction identification evaluation*

The identification procedure requires a covariance matrix, S, a hypothesis set, and initial estimates of conditional probabilities, $\Pr[\mu_j|\hat{\mathbf{F}}_k]$. Diagonal components of S serve as weighting factors, enabling the user emphasize particular components of the tire force vector in the selection algorithm. In the results that follow, S = diag(0.01 0.01 0.01 0.01 0.125 0.125), for pure braking and

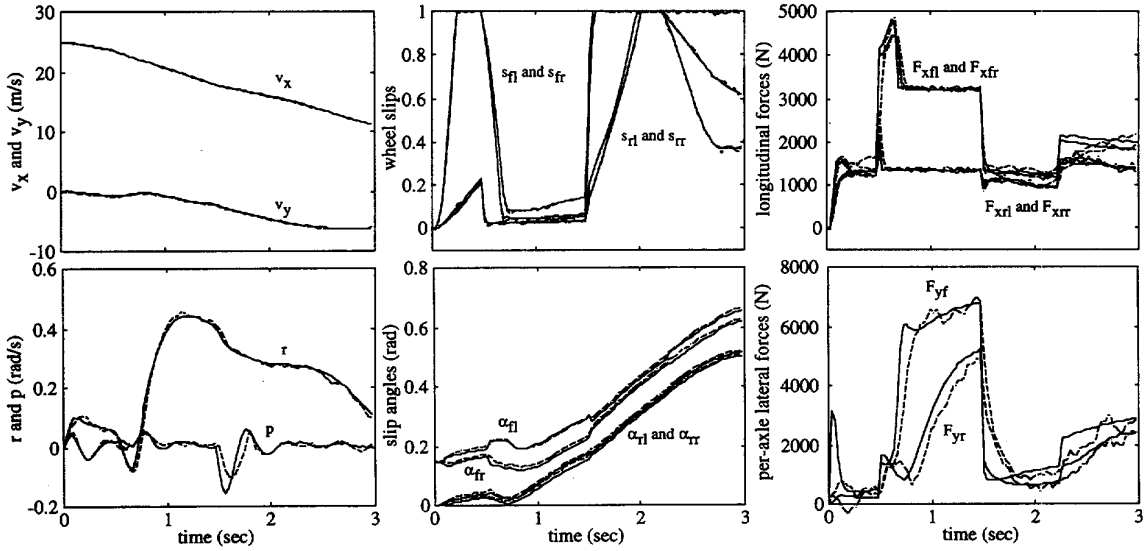

Fig. 4. Actual motion (solid) and state estimates (dashed) for $T_b = 3000$ N m, $\delta f_o = 0.15$ rad on a road surface with $\mu = 0.3$, [0,0.5) s, $\mu = 0.85$, [0.5,1.5) s, $\mu = 0.3$, [1.5,2.25) s, and $\mu = 0.5$, [2.25,3.0) s.

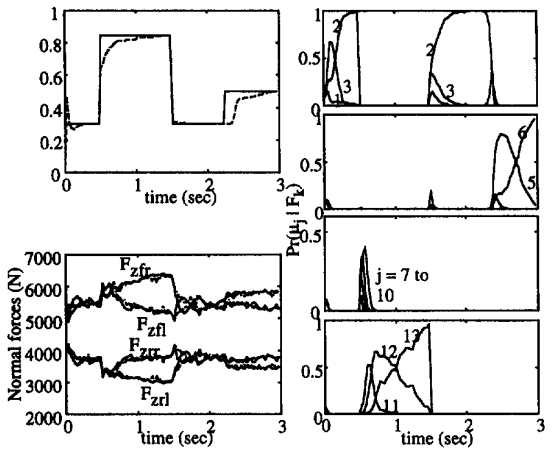

Fig. 5. Actual (solid) and estimated (dashed) μ and normal forces for the steering and braking inputs and road surface variations of Fig. 4. Conditional probabilities are given for each hypothesis 1 to 13, ($\mu = 0.25$ to $\mu = 0.85$).

combined maneuvers, placing equal emphasis on each on the longitudinal forces and slightly less emphasis on the per-axle lateral forces. $\mathbf{S}$ = diag(1 1 1 1 0.005 0.005) for pure steering maneuvers, placing more emphasis on lateral forces. The hypothesis set is μ = [0.25 to 0.85] in 0.05 increments. Computation burden per hypothesis is small, and a hypothesis set with small increments produced good results. Equal probability of each hypothesis being true was selected at $t = 0$, (i.e., no *a priori* knowledge of μ). Conditional probabilities were not allowed to drop below $\varepsilon = 0.00001$, enabling the algorithm to respond quickly to sudden changes in μ.

Figure 5 shows the μ estimate, normal forces, and $\Pr[\mu_j|\hat{\mathbf{F}}_k]$ histories for the trajectory of Fig. 4. Tracking of the actual road coefficient of friction is excellent. The $\Pr[\mu_j|\hat{\mathbf{F}}_k]$ histories show that the algorithm quickly converges to two hypotheses around the actual μ, while the remaining probabilities become small. The algorithm responds instantly when μ changes suddenly. Figure 6 shows the μ response for a variety of steering and braking maneuvers where actual values of μ match one of the hypothesized values (Fig. 6(a)–(d)) and where actual values of μ do not match one of the hypothesized values (Fig. 6(e)–(f)). In Fig. 6(a)–6(d), the estimated μ converges to the actual value in all except one case, and the worst case 5% settling time is 0.73 s. In Fig. 6(e)–6(f), μ settles to a hypothesized value just greater than or just less than the actual value; hence, the estimated μ is within $\pm$ 0.05 of the actual μ. The single case that does not converge is explained in the context of the tire force curves. In Fig. 6(a), the μ estimate approaches the actual value of μ, but does not converge to 0.85. Corresponding slip ratios are small (below 0.04). Fig. 1(a) shows that it is extremely difficult to distinguish curves of different μ at very small slip ratios, such as those in this maneuver; for slip ratios below approximately 0.04, the force–slip relationship is linear and is nearly independent of μ. Small "signal-to-noise" ratios in the state estimates in this region hinders μ identification. At higher slip ratios that are still well below that corresponding to peak longitudinal force, the information content in the estimates is sufficient, and the algorithm estimates μ accurately. The 5% settling time for

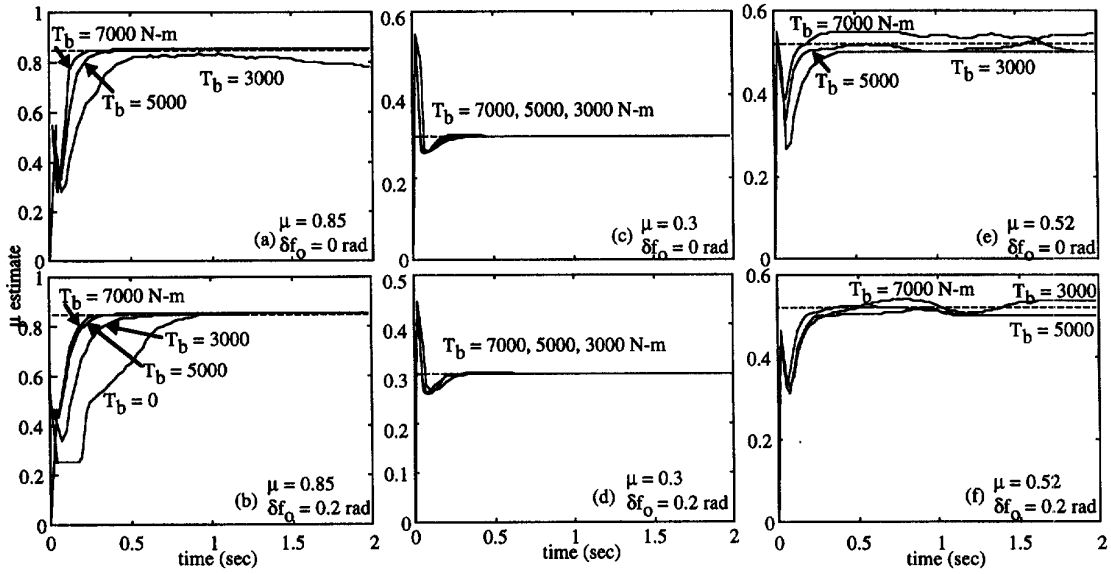

Fig. 6. Road coefficient of friction estimates for a variety of steering and braking inputs and actual road coefficients of friction. In a and d, the actual μ matches one of the hypotheses. In e and f, the actual μ does not match one of the hypotheses.

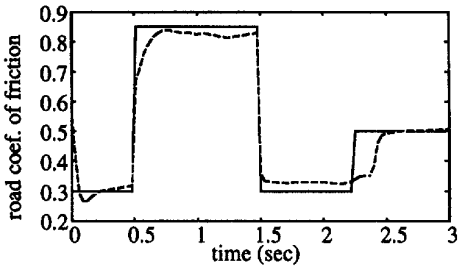

Fig. 7. Actual (solid) and estimated (dashed) μ for the inputs and road surface variations of Fig. 4. The vehicle model used in the μ identification algorithm does not match the actual vehicle.

the μ estimate and $T_b = 3000$ N m and $\delta f_o = 0.2$ rad is 0.35 s, well before slip ratios exceed peak slip value. μ identification for the pure steering maneuver exhibits the largest settling time largely because of a slow slip angle response. Fig. 1(b) shows that for small slip angles, it is also difficult to distinguish between μ hypotheses.

The μ identification procedure requires a vehicle model (for the EKBF) and tire force model. The tire force model is likely to be uncertain, as it depends on experimental and/or analytic modeling, and it can change over time with uncertain tire pressure and wear. In the results presented above, the tire force model used in the μ identification procedure was identical to the tire force model used to simulate vehicle motion. A robustness study was conducted by mismatching these two tire models. The tire force model of Szostak *et al.* (1988) includes parameters for several types of tires. Significant mismatch was introduced by selecting a tire for μ identification that did not match that of the actual vehicle. In addition, the vehicle load (m, I_{zz}, and cg location) assumed in the estimation model and actual vehicle were mismatched. Mismatch in vehicle load parameters was that produced by the difference between "driver only" and "fully loaded" conditions—approximately 5% difference in mass and moment of inertia, and a 20% change in cg location. State and tire force estimates are largely unaffected by the parameter uncertainty assumed. Figure. 7 shows the μ estimate for the trajectory of Fig. 4 for uncertain tire model and load parameters. Even in the face of uncertainty, the μ estimates converge to within one hypothesis of the actual value.

5.3. *Peak slip identification*

Figure 8 gives an example of the type of information that can be derived knowing μ. Here, the value of slip corresponding to peak longitudinal force, or "peak slip" is derived from a look up table given the EKBF slip-and-slip angle estimates, the static normal forces, and the μ estimate. The actual peak slip value and the estimated value are shown for each wheel. This information can be made available to an anti-lock braking system or a stability control system to determine controller setpoints that maximize stopping and/or lateral tire forces. Note also, that it is possible to estimate peak slip when inputs are severe enough to cause forces to exceed their peak values, as in Fig. 4, providing a means of verifying or updating the tire force model used for μ identification.

6. FIELD TEST DATA RESULTS

EKBF and μ identification were verified using field test data from a 1994 Ford Taurus GL, which were provided by VRTC for the following maneuvers: pure steering maneuvers at three fixed velocities, slowly increasing steering maneuvers at approximately constant velocity, pure braking maneuvers at several decelerations, and several miscellaneous open-loop hard steering/braking maneuvers. Occasionally, channels were bad or contained small biases or drift. When necessary, biases were removed from raw data by subtracting the average of 50 to 100 samples (0.5 to 1.0 s of data) prior to applying the control inputs; the same technique can be used if field test data were processed in real time. Data from known bad channels were not used. The following presents sample results of processing field test data.

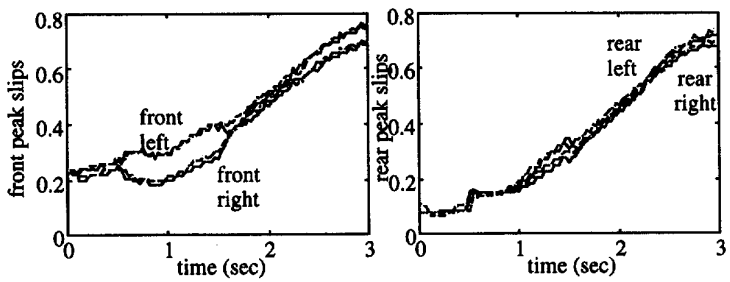

Fig. 8. Actual (solid) and estimated (dashed) peak slip for the inputs and road surface variations of Fig. 3.

6.1. *EKBF evaluation*

The EKBF was evaluated using field test data for fixed steering maneuvers (J-turns), fixed braking maneuvers, slowly increasing steering maneuvers, and combined maneuvers. Example results are presented here for fixed braking and fixed steering inputs. All field test data are for maneuvers conducted on dry asphalt, although the true underlying road friction is not known for these maneuvers.

Figure 9(a) shows example EKBF state and lateral tire force estimates for a $0.4g$ lateral acceleration J-turn at a velocity of 22 m/s (50 mph). As expected for the fixed input turn, the yaw rate reaches steady state, as do front and rear lateral force and slip angle estimates. The total lateral force divided by the vehicle mass (Fig. 9(a), a_y solid line) matches the measured acceleration well (dashed line) and measured yaw and roll rates

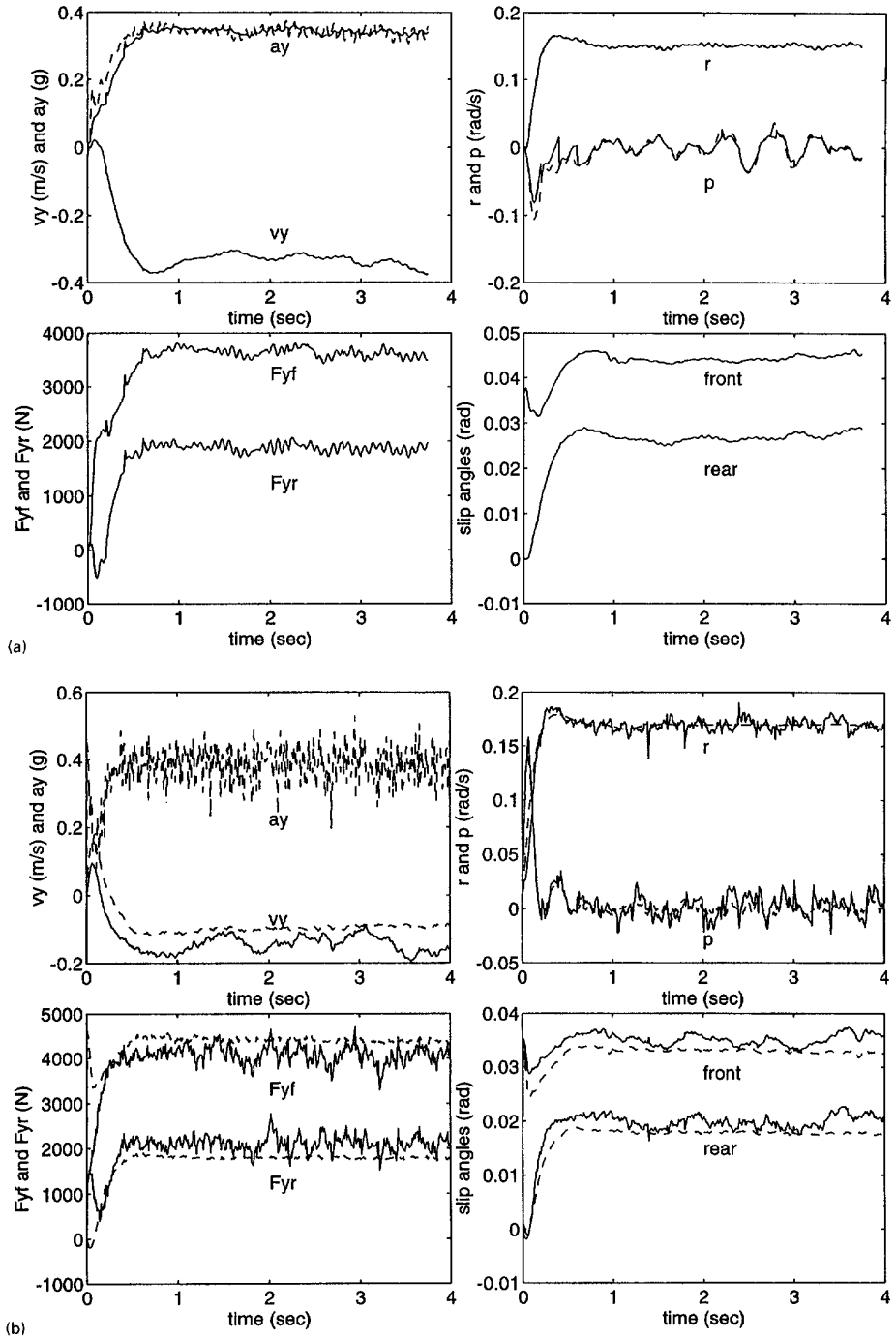

Fig. 9. EKBF results of processing (a) field test data and (b) simulation data for a $0.4g$ lateral acceleration J-turn at 22 m s^{-1} (50 mph). Solid line gives state estimates. In (a) dashed lines gives measured data, and in (b) dashed lines give actual motion.

match estimated yaw and roll rates well. However, because forces and slip angles cannot be measured, it is difficult to evaluate EKBF results directly to determine whether the entire state and individual force and slip angle estimates are reasonable. For qualitative comparison, the same maneuver was simulated using an eight-degree-of-freedom model of the test vehicle and the analytic tire force model on a $\mu = 0.83$ road surface. Figure 9(b) shows the simulation and estimation results for this comparable maneuver. Simulation data appear "noisy" due to simulated random disturbance inputs. Forces and state histories estimated using simulation data match field test data results reasonably well. The transient behavior of the state estimates for both field test data and simulation data is similar. The simulated maneuver gives slightly higher steady-state lateral forces and yaw rate, and the corresponding slip angles are smaller. This indicates that the road friction underlying the field test data may be smaller than $\mu = 0.83$ used in the simulation, or the tire force model used in the simulation does not exactly match the actual vehicle's tires.

Figure 10 shows EKBF results of processing field test data for a $0.31g$ braking maneuver along with simulation results for the same inputs on a $\mu = 0.88$ surface. The estimated forces from processing field test data match the simulated forces very well, although again, process noise injected into the simulation makes the corresponding force and slip estimates appear noisy, compared to test data results. Wheel slip estimates are small for this modest braking maneuver; however, they are reasonable when compared to the simulation results. Figure 11 shows EKBF results for a hard braking maneuver, along with corresponding results for simulation of the same maneuver on a $\mu = 0.88$ surface. Here, the braking input is severe enough to activate the vehicle's ABS system, as reflected by cycling in the force and slip estimates. The vehicle operates at maximum deceleration ($a_x = 0.9g$). The simulation shows somewhat different behavior, with rear wheel lock occurring for the inputs considered, and slightly smaller deceleration. This again indicates that the vehicle simulation model, road friction assumed, tire model, and/or brake model contains error. However, comparison of the performance of the EKBF for simulation with EKBF results for field test data indicates excellent tracking of individual longitudinal tire forces during severe maneuvering.

6.2. *Tire force modeling*

Data such as those presented in Figs. 9–11 can be used to extract or verify tire force models that provide forces as functions of wheel slip, slip angle, normal force, and road friction. For example, a pure braking maneuver gives longitudinal force vs slip at approximately constant normal force and zero slip angle. Figures 12 and 13 give examples of such data for the severe braking maneuver of Fig. 11. Here, the inputs cause slip ratios at both wheels to exceed a value corresponding to peak longitudinal force. For the field test data, when the peak is exceeded, the braking system cycles, tracing the longitudinal force vs slip characteristic in the nonlinear regime of the tire force curves. Some scatter exists due to noise, disturbances, and normal force variation. Figure 14 shows per-axle lateral force estimate vs slip angle estimate based on EKBF results of processing field test data and

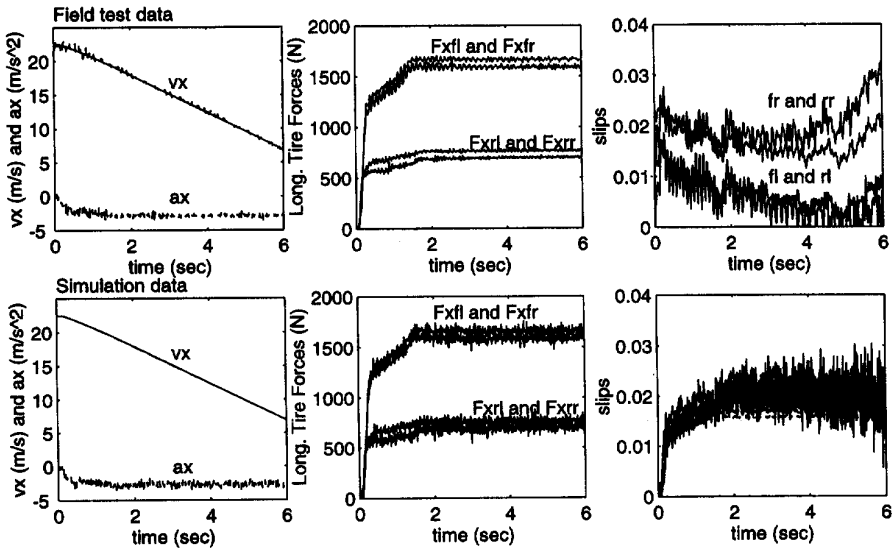

Fig. 10. EKBF results of processing (a) field test data (top) and (b) simulation data (bottom) for a $0.31g$ braking maneuver. Solid line gives state estimates. In (a) dashed lines gives measured data, and in (b) dashed lines give actual motion.

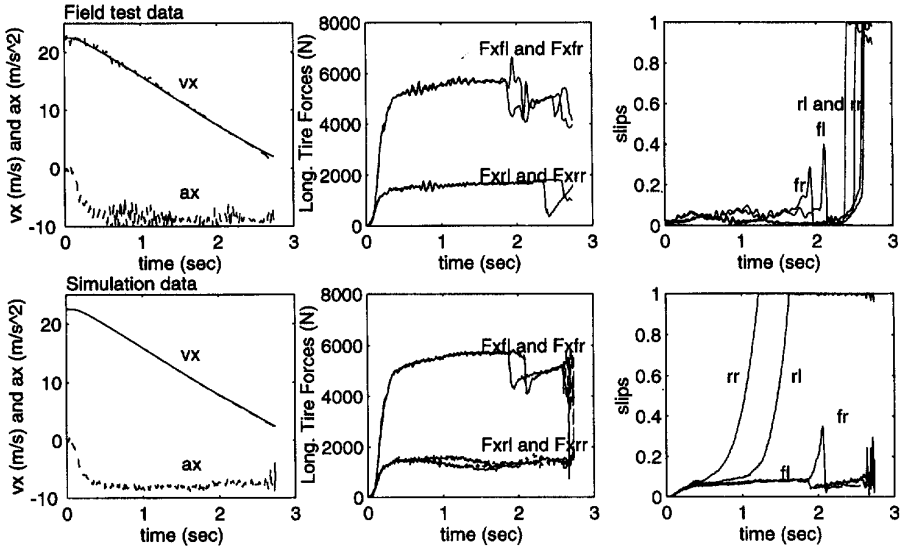

Fig. 11. EKBF results of processing (a) field test data (top) and (b) simulation data (bottom) for a hard braking maneuver (ABS active). Solid line gives state estimates. In (a) dashed lines gives measured data, and in (b) dashed lines give actual motion.

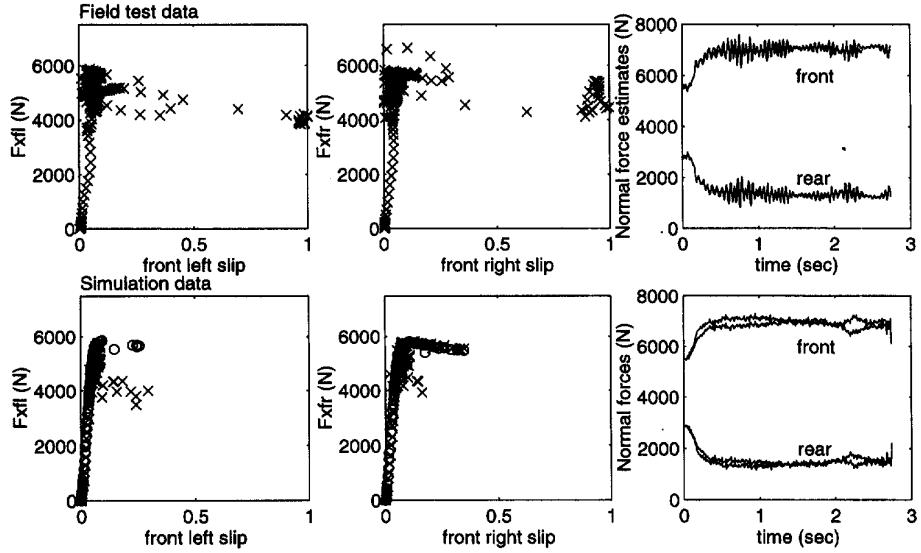

Fig. 12. Front wheel longitudinal force vs slip for the braking maneuver of Fig. 11. '×' represents data based on state estimates, 'O' (bottom plots) represents "true" tire forces generated for simulation.

simulation data for a slowly increasing steer input. Cornering stiffness can be estimated from lateral force vs slip angle data, since slip angle varies approximately linearly with time for the slow steer maneuver.

Tire force data presented in Figs. 12–14 are based on single maneuvers. Careful selection of and repeated maneuvers for identical inputs can produce sufficient data for regression analysis in order to build or verify a tire force model. Data from Figs. 12 and 13 can be used to determine F_x vs slip at approximately constant normal force and zero slip angle, while Fig. 14 data can be used to determine F_y vs slip angle at approximately zero slip and constant normal force. Example results of regression analysis are shown in Table 3 for the linear region of the tire force curves. Also shown in Table 3 are slopes of F_x/F_z vs slip at zero slip angle and F_y/F_z vs slip angle at zero slip based on machine tire tests of the test vehicle's tires. Normal forces associated with machine tests do not match normal forces generated during field test maneuvers; therefore, results cannot be compared directly. Nevertheless, cornering stiffness from field test data follows the same trend with increasing normal force as cornering stiffness determined from machine test

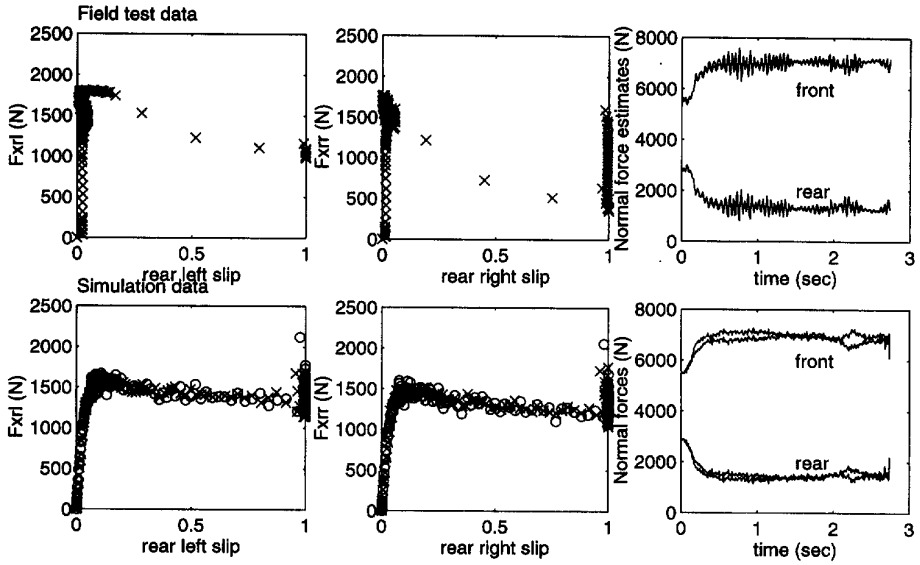

Fig. 13. Rear wheel longitudinal force vs slip for the braking maneuver of Fig. 11. '×' represents data based on state estimates, '○' (bottom plots) represents "true" tire forces generated for simulation.

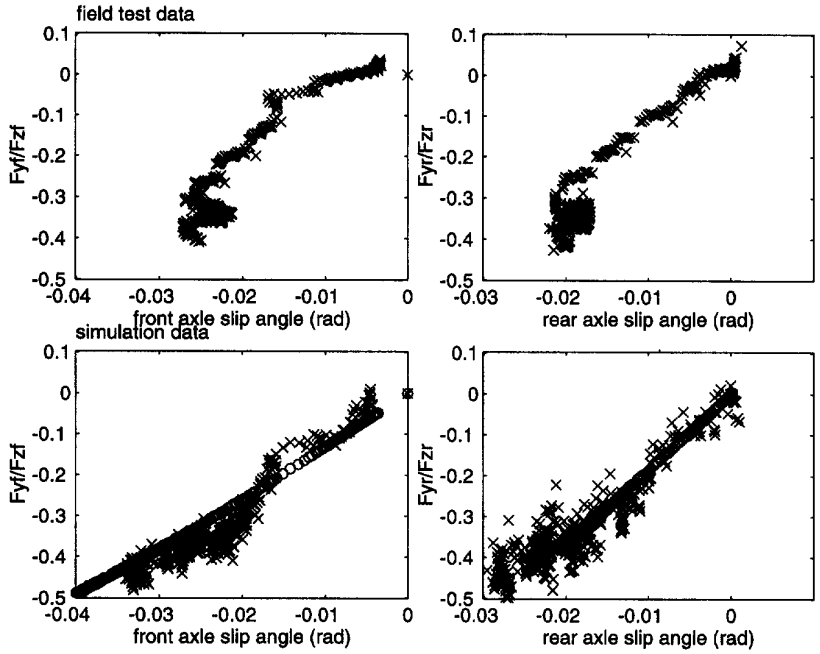

Fig. 14. Lateral force vs slip angle for a slow steer maneuver. '×' represents data based on state estimates, '○' (bottom plots) represents "true" tire forces generated for simulation.

data. Longitudinal force characteristics determined from field test vary significantly with normal force, while machine test data do not reflect a similar trend.

6.3. *Road friction identification evaluation*

The effectiveness of road friction identification depends on the magnitude of the tire forces; for very small inputs, the forces are small and nearly independent of road friction. Severe inputs generate large tire forces that enhance friction identification. Figure 15 shows the road friction estimate for a severe braking/steering maneuver ($a_x = 0.9g$ peak, and $a_y = 0.8g$ peak). The hypothesis set for this task was $\mu = 0.3$ to 0.9 in increments of 0.05. Underlying road friction for the simulation is 0.88, and the estimate converges to 0.9. While the underlying road friction for the field test data is unknown, the

Table 3. Comparison of tire data from field testing to flat-trac II machine test data

Longitudinal:	Slop of F_x/F_z vs slip	
Field test data	Avg.F_z(N)	Slop (N/N/rad) and 95% conf. intervals
Fig. 13 rear left	1330	38.95 ± 3.23
Fig. 13 rear right	1330	41.08 ± 4.42
Fig. 12 front left	7050	15.01 ± 0.91
Fig. 12 front right	7050	16.47 ± 1.37
Flat Trac data		
Pulse-brake	2500	18.98 ± 0.43
Pulse-brake	4180	19.80 ± 0.33
Pulse-brake	5810	19.40 ± 0.38
Lateral:	Slop of F_y/F_z vs slip angle	
Field test data†	Avg.F_z(N)	Slop (N/N/rad) and 95% conf. intervals
Fig. 14 rear	2690	17.42 ± 0.23
Fig. 14 front	5330	13.12 ± 0.26
Flat Trac data		
Quasi-static steer	2495	16.44 ± 0.43
Quasi-static steer	4140	13.93 ± 0.30
Quasi-static steer	5790	11.92 ± 0.32

†For lateral force vs slip angle, field test data results are based on per-axle lateral force and per-axle (average of left and right wheel) slip angle estimates.

value also converges to $\mu = 0.9$. This estimate is comparable to measured road friction from Ebert (1989), which reports a mean value of 0.89 and standard deviation of 0.055 for peak coefficient on dry test surfaces, based on 38 samples. In Fig. 15, estimated road friction settles to within 5% of the steady-state value in less than 1.5 s. Figure 16 shows road friction estimates for pure braking ranging from the $0.31g$ maneuver of Fig. 10 to the maximum deceleration maneuver of Fig. 11. As the severity of braking increases, tire forces become more nonlinear, providing a larger signal-to-noise ratio to determine road friction; hence, the transient response of the estimate improves. For braking below $0.31g$, the algorithm is unable to positively determine road friction.

While the road friction estimation procedure works well for combined maneuvers, and braking greater than $0.31g$, it is extremely difficult to determine road friction based on pure steering input data; lateral force vs slip angle is nearly independent of μ at very small slip angles such as those produced for $0.2g$ and $0.4g$ J-turn maneuvers. Simulation results presented earlier indicate that modest combined braking and steering inputs provide sufficient information content to identify road friction. No modest combined input test data were available for this study. In addition, data were available only for tests conducted on dry asphalt. Future research includes processing of field test data for modest steering and braking maneuvers as well as data for other road surfaces.

7. COMPUTATION REQUIREMENTS

The EKBF requires 131 K floating point operations (FLOPS) per sample time to propagate the

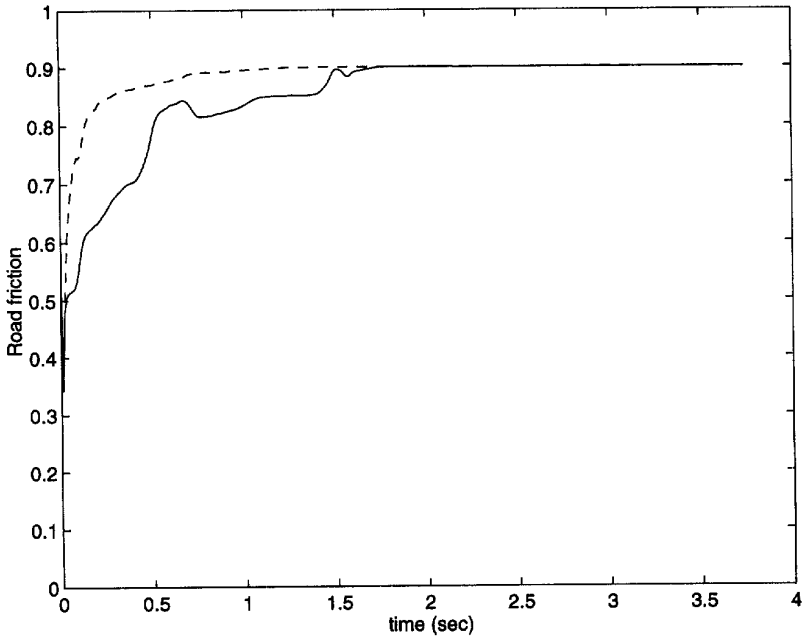

Fig. 15. Road friction estimate for a hard braking/steering maneuver. For simulation data (dashed line), the actual road friction is 0.88. For field test data (solid line), the underlying road friction is unknown.

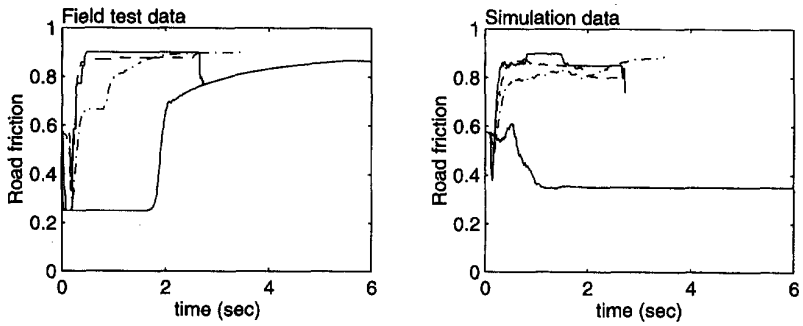

Fig. 16. Road friction estimates for pure braking with $a_x = 0.31$ (solid), 0.51 g (dash-dot), 0.76 g (dashed), and 0.9 g (solid).

state estimate (9 nonlinear and 12 linear equations) and the 21×21 covariance matrix using numerical integration. The μ identification algorithm requires 600 FLOPS per sample time per hypothesis. For 13 hypotheses, a total of 139 K FLOPS per sample time are required to implement the EKBF and μ identification. Sample times of 0.025 and 0.03 s were used to generate the results in this paper, and sample times up to 0.1 s did not cause integration instability or unacceptable degradation in the state estimates or μ identification results. For such sample times and computation speeds, a 1.4 to 5.6 MFLOP processor is required. The computation burden was determined without attempting to introduce efficient algorithms in the EKBF; since the covariance matrix is symmetric, the covariance propagation can be modified to incorporate computation reducing algorithms.

8. CONCLUSIONS

The results of extended Kalman–Bucy filtering and road friction identification for an eight-degree-of-freedom vehicle show excellent tracking and robustness properties. The EKBF state estimates follow the actual state well, even in the face of abrupt changes in road conditions. In simulation results, tracking of the μ estimate is excellent, and the μ identification procedure gives good convergence for a broad range of inputs. The robustness study indicates that the μ identification procedure can accommodate reasonable uncertainty in the tire force and vehicle models. The methods presented here give state estimates that can be used for advanced feedback control and road coefficient of friction estimates that can be used to determine controller setpoints and to make intelligent driving decisions.

The results of processing field test data support simulation results. Performance of the filter for field test data is comparable to performance for simulation data, and the EKBF works well for a maneuvers ranging from modest to severe. The resulting state estimate histories can be used to generate data for construction or verification of tire force models. For the EKBF, prior knowledge of tire properties or road conditions is not required. Sensor requirements are reasonable and are typical of modern testing facilities. Road friction identification for field test braking maneuvers and for a combined hard steering/braking maneuver produced results that are consistent with measured road friction for dry asphalt at typical test facilities.

Throughout the results presented, the difference between tire forces and wheel slip from right to left is small, indicating that it is possible to use a per-axle vehicle model in the EKBF. This would further reduce computation. Also, the results indicate that for severe maneuvers, it is possible to identify peak slip from force and slip estimates without knowing μ. This provides a means of verifying and/or updating the tire force model used in the μ identification procedure. With minor modification, the μ estimation procedure can be used to determine when a vehicle is on a split-μ surface, if the eight-degree-of-freedom vehicle model and estimation of individual longitudinal forces are retained. These variations, along with additional robustness studies, experimental verification of road-friction identification on other road surfaces, and use of the algorithm in feedback control systems are the subject of future research.

Acknowledgements—This research was supported by the National Research Council Transportation Research Board under the IDEA program, contract No. IVHS-14. The author also thanks Mr. Jeff Chrstos and VRTC for providing field test data.

REFERENCES

Allen, R. W., H. T. Szostak and T. J. Rosenthal (1986). Test methods and computer modeling for the analysis of ground vehicle handling. *Society of Automotive Engineers*, Paper No. 861115.

Constantine, C. J., J. E. Bowman, and E. H. Law (1991). Development of models and computer programs for lateral dynamics of automobiles during combined steering and braking maneuvers. TR-90-132-ME-MMS, Mechanical Engineering Department, Clemson Univ.

Ebert, N. (1989). SAE tire braking traction survey: a comparison of public highways and test surfaces. SAE Paper No. 890638.
Pape, D. (1996). Dynamic vehicle simulation to evaluate countermeasure systems for single vehicle roadway departures. *Society of Automotive Engineers*, Paper No. 960517.
Ray, L. R. (1995). Nonlinear state and tire force estimation for advanced vehicle control. *IEEE Trans. Control Systems Technol.*, **3**, 117–124.
Stengel, R. F. (1986). *Stochastic Optimal Control:: Theory and Application*. Wiley, New York.
Szostak, H. T., R. W. Allen and T. J. Rosenthal (1988). Analytical modeling of a driver response in crash avoidance maneuvering, Vol II: an interactive tire model for driver/vehicle simulation. U.S. DOT, Report No. DOT HS 807-271.
Taheri, S. and E. H. Law (1990). Investigation of a combined slip control braking and closed loop four wheel steering system for an automobile during combined hard braking and severe steering. *Proc.* 1990 *American Control Conf.*, San Diego, CA, May 1990.